Hindawi
Wireless Communications and Mobile Computing
Volume 2022, Article ID 3018225, 13 pages
https://doi.org/10.1155/2022/3018225

Research Article

On the Power-Splitting Relaying Protocol for SWIPT with Multiple UAVs in Downlink NOMA-IoT Networks

Huu Q. Tran,[1] **Ca V. Phan**,[2] **and Quoc-Tuan Vien**[3]

[1]*Industrial University of Ho Chi Minh City, Vietnam*
[2]*Ho Chi Minh City University of Technology and Education, Vietnam*
[3]*Middlesex University, UK*

Correspondence should be addressed to Huu Q. Tran; tranquyhuu@iuh.edu.vn

Received 23 November 2021; Revised 5 July 2022; Accepted 27 July 2022; Published 5 September 2022

Academic Editor: Xin Liu

Unmanned aerial vehicle (UAV) communication and non-orthogonal multiple access (NOMA) are two promising technologies for wireless 5G networks and beyond. The UAVs can be used as flying base stations to form line-of-sight communication links to the Internet of things devices (IDs) and to enhance the performance of usual terrestrial cellular networks. Moreover, the UAVs can also be deployed as flying relay nodes for forwarding data from a base station (BS) to the IDs. On the other hand, non-orthogonal resource sharing for many concurrent users is exploited in NOMA, thus improving spectrum efficiency (SE) and supporting massive connections. The NOMA combined with energy harvesting (EH) in an amplify-and-forward (AF) with cooperative UAV systems is researched. Specifically, the UAVs act as rotary-wing relays to forward data from the BSs to two IDs. This paper focuses on the analysis of outage probabilities (OPs), system throughput, and energy efficiency (EE) for two IDs. Besides, we also do the asymptotic analysis of OPs at high signal-to-noise ratios (SNRs). Furthermore, this paper also inspects the impacts of the UAV-based relaying on the OP, system throughput, and EE of the proposed NOMA scheme. The derived asymptotic expansions show that the suggested model can enhance user fairness and the analytical results match the simulation results.

1. Introduction

Unmanned aerial vehicles (UAVs) communications and non-orthogonal multiple access (NOMA) are envisioned as two key technologies for unlocking the potential of the fifth-generation (5G) and future networks[1, 2]. In particular, the use of UAVs for 5G and beyond-5G networks has received much attention over the past few years [3]. Owning to distinctive characteristics, UAVs have been adopted for a variety of wireless networks and communication applications, for example, UAV-carried flying base stations (BSs) for capacity and coverage improvement, public safety scenarios, information dissemination, UAV-based wireless backhaul, and cellular connected UAVs as mobile users [4]. The NOMA technique exhibits benefits such as increased user data rate, massive connectivity, reduced end-to-end latency, improved fairness among users, high spectral efficiency (SE), and more energy efficiency (EE) than that of traditional orthogonal multiple access (OMA) [5–11]. The NOMA exploited two mechanisms including superposition coding (SC) and successive interference cancellation (SIC) [12, 13]. Some recent studies have showed that the integration of NOMA into UAV networks can enhance the network performance in terms of max-min rate [14], sum rate [15], and mission completion time [16], over conventional OMA schemes. Two protocols are exploited for energy harvesting (EH) at relays including power splitting relay and time switching relay in the decode-and-forward (DF) cooperative communication network [17, 18]. NOMA in UAV-enabled cooperative amplify-and-forward (AF) with the outdated relay selection algorithm is investigated [19].

1.1. Related Works. In this section, we review the novel study works on NOMA and UAV networks. UAV-assisted communication has become a potential application in industry and academic fields. NOMA is one of the important candidates to integrate UAV into 5G and future networks due to its overwhelming characteristics, such as superior spectral efficiency, low latency, and massive connectivity [2]. UAVs have also been recently studied as a promising solution to proven their potential in civil applications such as aerial photography, enhanced freight distribution, and wildfire management and disasters [4, 20]. A resource allocation scheme was proposed in NOMA UAV communication to enhance the user transmission rate with worse channel state information (CSI) [21]. UAVs can act as moving BSs or relays to facilitate reliable and efficient communication with multiple users [22, 23]. In [24], the authors discussed NOMA-based UAV-aided communications such as UAV-BS-enabled NOMA and NOMA-assisted cellular-connected UAVs. In [25], the authors conducted the complete performance analysis of a NOMA-aided UAV communication system, including selection combining double diversity receivers on UAVs, communicating over bivariate Rician shadowed fading channels. The work in [26] investigated the impact of residual hardware impairments on the performance of UAV-aided NOMA multiway relay networks by deriving the approximate analytical expressions for the achievable sum rate. Specifically, the asymptotic analysis in the high signal-to-noise-ratio (SNR) regions is carried out by invoking a high SNR slope and high SNR power offset. In [27], the authors investigated the impact of residual hardware impairments on the performance of UAV-aided NOMA multiway relay networks by deriving the approximate analytical expressions for the achievable sum rate. Specifically, the asymptotic analysis in the high signal-to-noise-ratio (SNR) regions is carried out by invoking a high SNR slope and high SNR power offset. In [28], the authors studied a 5G-based IoT to access the 5G spectrum to transfer 5G and IoT information simultaneously. The 5G network can be used at the IoT nodes to transmit voice and video information while using the IoT network for forwarding sensing data.

The work presented in [29] investigated a novel UAV relay-assisted IoT model with the emergency communication system that takes into account the latency requirement of Internet of Things (IoT) devices and the limited storage capacity of the UAV. A novel joint content caching and EH scheme is studied to improve UAV communications in the IoT NOMA network wherein a UAV acts like an aerial relay for serving users on demand [30]. In [31], the authors studied the throughput maximization problem with a focus on UAV-assisted wireless communication, considering a communication system with one couple of source and destination, where a UAV serves like an aerial relay based on an AF scheme and EH using a PS protocol. Performance of the IoT system with an EH UAV-enabled relay with downlink NOMA under Nakagami-m fading using the DF and AF schemes is investigated, where the time switching and adaptive power splitting protocols are utilized for the UAV [32].

Based on the above review, in this paper, we focus on power-switching relaying (PSR) for an RF EH and AF-based multiple-UAV NOMA in a SWIPT IoT system.

1.2. Motivation and Contribution. This paper researched the engagement of EH and AF-based multiple-UAV NOMA in a SWIPT IoT system wherein a UAV serves as a rotary-wing relay to communicate with two IoT devices (IDs). We also look at the UAV option (UAVO) scheme because it requires CSI knowledge of one-hop links. Hence, the use of rotary-wing relay AF in the UAVO model is greatly desirable in practice when complicated problems occur as the main anxiety. According to the depicted system model, the outage probabilities (OPs), the system throughput, and EE of the NOMA schemes in AF transition systems with UAVO were studied. The major contributions of this paper are outlined as follows:

(i) We exploit NOMA access technology in a dual-hop network to improve the SE of the network

(ii) A system model is studied in this work that consists of a BS and n types of UAVs and two IDs

(iii) The use of one SWIPT based EH and information processing (IP) protocol, specifically BS-based PSR, is exploited at a UAV that serves as a rotary-wing relay in this model

(iv) We derive closed-form expressions of OPs, system throughput, and EE at two IDs to assess the performance of the PRS scheme in SWIPT based on multiple-UAV cooperative NOMA systems

1.3. Organization. The remainder of the paper is arranged as below: Section 2 shows the proposed system model and assumptions. Section 3 analyzes the performance parameters with OP, throughput, and EE of the system. Section 4 discusses the simulation results. Ultimately, Section 5 is the main conclusion.

2. System Model

We investigate a downlink cooperative two-hop rotary-wing relay system in which a base station (BS) aims to send the signal to two IDs, i.e., D_1 and D_2 with the support of one out of N AF UAVs $(UAV_1, UAV_2, \cdots, UAV_N)$ with $N > 1$, as shown in Figure 1. It is assumed that there is no communication between the UAVs. We mainly focus our attention on a homogeneous network topology in which all wireless links show non-selective Rayleigh block fading and additive white Gaussian noise (AWGN).

As shown in Figure 1, without loss of generality, we assume that the channels of two IDs have been ordered as $h_{SD_1} \leq h_{SD_2}$. We also investigate that D_1 and D_2 are coupled together to implement NOMA downlink cooperative system. Hence, two successive phases are implicated for completing the information transmission that can be combined by selection combining. Selection combining (SC): Out of the N signal received, the strongest signal is selected. When

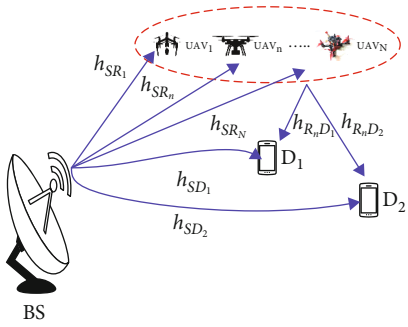

Figure 1: System model.

signal N is independent and distributes Rayleigh, the increase is shown in the power ratio as follows $\sum_{n=1}^{N}(1/n)$.

Table 1 below lists the parameters used throughout the paper, unless otherwise stated.

2.1. BS-Based PSR Protocol of EH at UAV_n. At the UAV_n, we consider the EH mechanism BS-based PSR protocol.

Figure 2 depicts a diagram illustration of BS-based PSR scheme for EH at UAV_n in the block time of T.

For direct link: In the whole time, T, BS transmits information directly to two IDs D_1 and D_2, with transmission powers $P_{S_1}=P_{S_2}=P_S$.

For indirect link: The collected signal power at UAV_n is indicated by P. Assuming that the BS transmits the information to UAV_n in the half-block of T, while the information is sent from UAV_n to two IDs D_1 and D_2 in the remaining time of T (i.e., $T/2$). BS concurrently sends the superposed coding signal to R_n. Therefore, the sent signal at BS can be given by

$$x_{BS} = \sqrt{a_1 P_S}x_1 + \sqrt{a_2 P_S}x_2, \tag{1}$$

Based on the employment of superposition of the sent signals at BS like in the NOMA scheme, the surveillance at UAV_n can be given by

$$\begin{aligned} y_{UAV_n} &= h_{SUAV_n}x_{BS} + n_{UAV_n} \\ &= h_{SUAV_n}\left(\sqrt{a_1 P_S}x_1 + \sqrt{a_2 P_S}x_2\right) + n_{UAV_n}. \end{aligned} \tag{2}$$

The signals received at two IDs D_1 and D_2, respectively, are given by

$$y_{D_1} = h_{SD_1}\left(\sqrt{a_1 P_S}x_1 + \sqrt{a_2 P_S}x_2\right) + n_{D_1}, \tag{3}$$

$$y_{D_2} = h_{SD_2}\left(\sqrt{a_1 P_S}x_1 + \sqrt{a_2 P_S}x_2\right) + n_{D_2}. \tag{4}$$

Since D_1 is further to UAV_n than D_2, the power is allocated for D_1 more than that for D_2 to ensure the user fairness.

With no generality losses, $0 < a_2 < a_1$ satisfies $a_1 + a_2 = 1$. Based on PSR protocol, UAV_n divides the collected power into two portions consisting of collected energy and IP energy. The energy harvested at UAV_n is obtained by

$$EH = P_S\left|h_{SR_n}\right|^2\eta\beta\left(\frac{T}{2}\right), \tag{5}$$

where η relies on the rectifier and the EH circuitry at UAV_n. The total energy harvested in the EH phase is consumed at UAV_n while forwarding the decoded signal to D_i, $i \in \{1, 2\}$. The transmission power at UAV_n depends on EH and is determined by

$$P_{Rn} = \frac{EH}{(T/2)} = P_S\left|h_{SR_n}\right|^2\eta\beta = P_S.G_E, \tag{6}$$

where $G_E = |h_{SR_n}|^2\eta\beta$ indicates the EH coefficient in the PSR protocol.

2.2. Information Processing at UAV_n and D_i. In the first phase, BS transmits signals x_1 and x_2 for all UAVs and two IDs as in Equation (1).

During the second phase, UAV_n transmits the signal $x_{R_n} = G_n y_{R_n}$ to two IDs D_1 and D_2, where G_n denotes the amplifying gain at UAV_n, i.e.,

$$G_n^2 = \frac{P_{UAV_n}}{P_S\left|h_{SUAV_n}\right|^2 + N_0} = \frac{\rho G_E}{Y_n + 1}, \tag{7}$$

where $\rho\Delta = P_S/N_0$ depicts the sent SNR and the random variables (RVs) $A_i = \rho|h_{SD_i}|^2$, $B_n = \rho|h_{SUAV_n}|^2$, and $C_{\text{in}} = \rho|h_{UAV_nD_i}|^2$ describe the instantaneous SNRs of the links BS $\longrightarrow$ D_i, BS $\longrightarrow$ R_n, R_n $\longrightarrow$ D_i, respectively. Thus, the signals at D_1 and D_2 are forwarded by UAV_n and can be given by as follows:

$$\begin{aligned} y_{UAV_nD_1} = h_{UAV_nD_1}x_{UAV_n} + n_{UAV_nD_1} &= G_n h_{UAV_nD_1}h_{SUAV_n}\sqrt{a_1 P_S}x_1 \\ &+ G_n h_{UAV_nD_1}h_{SUAV_n}\sqrt{a_2 P_S}x_2 \\ &+ G_n h_{UAV_nD_1}n_{UAV_n} + n_{UAV_nD_1}, \end{aligned} \tag{8}$$

$$\begin{aligned} y_{UAV_nD_2} = h_{UAV_nD_2}x_{UAV_n} + n_{UAV_nD_2} &= G_n h_{UAV_nD_2}h_{SUAV_n}\sqrt{a_1 P_S}x_1 \\ &+ G_n h_{UAV_nD_2}h_{SUAV_n}\sqrt{a_2 P_S}x_2 \\ &+ G_n h_{UAV_nD_2}n_{UAV_n} + n_{UAV_nD_2}. \end{aligned} \tag{9}$$

During the first phase, consider x_2 like interference in y_{D_1}. The immediate SINR at D_1 is provided by

$$\gamma_{1,D_1} = \frac{a_1\rho\left|h_{SD_1}\right|^2}{a_2\rho\left|h_{SD_1}\right|^2 + 1} = \frac{a_1 A_1}{a_2 A_1 + 1}. \tag{10}$$

Table 1: Notation description.

Notation	Description
$h_{SUAV_n} \sim \mathcal{CN}(0, \Omega_{SUAV_n})$	The complex flat coefficient between BS and UAV_n
$n_{UAV_n} \sim CN(0, N_0)$	Additive white Gaussian noise (AWGN) at UAV_n
$h_{UAV_nD_i} \sim \mathcal{CN}(0, \Omega_{UAV_nD_i})$	The complex flat coefficient between UAV_n and D_i, $i \in \{0, 1\}$
$n_{UAV_nD_i} \sim CN(0, N_0)$	Additive white Gaussian noise (AWGN) at D_i indirect link between BS and D_i
$h_{SD_i} \sim \mathcal{CN}(0, \Omega_{SD_i})$	The complex flat coefficient with direct link between BS and D_i
$n_{D_i} \sim CN(0, N_0)$	Additive white Gaussian noise (AWGN) at D_i with direct link between BS and D_i
P_S	Transmission power at the BS
$\beta(0 < \beta < 1)$	The power splitting ratio at the UAV_n
$E[.]$	Expectation operation
$E\left[\left\|n_{UAV_nD_i}\right\|^2\right] = N_0$	Expectation operation of AWGN at UAV_n
m	The path-loss of channel model
$x_i(i \in \{0, 1\})$	The transmitted signals from $BS \longrightarrow UAV_n \longrightarrow D_i$ indirect link between BS and D_i and $BS \longrightarrow D_i$ with direct link between BS and D_i
$E\left[\left\|x_i\right\|^2\right] = 1.$	Expectation operation of x_i
T	The total time block
a_1	Power allocation coefficient for signal x_1
a_2	Power allocation coefficient for signal x_2
$\eta(0 < \eta \leq 1)$	The energy conversion efficiency at the UAV_n

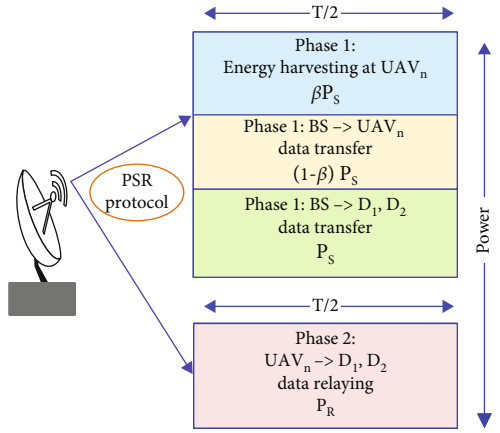

Figure 2: Diagram illustration of PSR-based UAV_n.

In the same way, the instantaneous SINR at D_2 is provided by

$$\gamma_{1,D_2} = \frac{a_1\rho\left|h_{SD_2}\right|^2}{a_2\rho\left|h_{SD_2}\right|^2 + 1} = \frac{a_1A_2}{a_2A_2 + 1}. \tag{11}$$

By following the NOMA scheme, D_2 decrypts the message specified for D_1 first and deletes it with SIC; then, it decrypts itself without interfering. Hence, the immediate SNR at D_2 is provided by

$$\gamma_{2,D_2} = a_2A_2. \tag{12}$$

During the second phase, the instantaneous SINR calculation is same as the first phase. Therefore, the immediate SINR at D_1 relative to the link is expressed as

$$\gamma_{UAV_nD_1} = \frac{a_1G_EB_nC_{1n}}{a_2G_EB_nC_{1n} + G_EC_{1n} + B_n + 1}, \tag{13}$$

$$\gamma_{UAV_nD_{12}} = \frac{a_1G_EB_nC_{2n}}{a_2G_EB_nC_{2n} + G_EC_{2n} + B_n + 1}, \tag{14}$$

$$\gamma_{UAV_nD_2} = \frac{a_2G_EB_nC_{2n}}{G_EC_{2n} + B_n + 1}. \tag{15}$$

Finally, by using (10)-(15), it is assumed that the signals from the forward link and the direct link are associated by selection combining (SC). The instantaneous SINR per ID can be written as

$$\gamma_{D_1} = \max\left(\gamma_{1,D_1}, \gamma_{UAV_nD_1}\right), \tag{16}$$

$$\gamma_{D_2} = \max\left(\gamma_{1,D_2}, \gamma_{UAV_nD_2}\right). \tag{17}$$

In the next, we will compute the OPs of two IDs assuming a UAVO method [33]. Therefore, the transition index is chosen and its corresponding SNR is given by

$$n* = \arg\max_{n=1,\cdots,N} \gamma_{BSUAV_n}, B_{n*} = \max_{n=1,\cdots,N} B_n, \tag{18}$$

in which the instantaneous SNR at UAV_n is denoted by $\gamma_{BSUAV_n} = B_n$.

3. Performance Analysis

3.1. Outage Performance. The target SINR of two IDs is determined by the ID's request for the quality of service (QoS). Hence, each ID has a target SINR, $\gamma_{th_i} = 2^{2R_i} - 1, i \in \{1, 2\}$ [3, 5].

3.1.1. Outage Probability at D_1. Based on [4], the RVs' cumulative distribution functions (CDF) and, correspondingly, can be expressed by

$$F_{A_i}(\gamma_{thi}) = 1 - \exp\left(-\frac{\gamma_{thi}}{\Omega_{A_i}}\right), \tag{19}$$

$$F_{B_{n*}}(\gamma_{th_i}) = \left(1 - \exp\left(-\frac{\gamma_{th_i}}{\Omega_{B_n}}\right)\right)^N = 1 - \sum_{n=1}^{N} \binom{N}{n} (-1)^{n-1} \exp\left(-\frac{\gamma_{thi}}{\Omega_{B_n}}\right), \tag{20}$$

$$F_{C_{\text{in}*}}(\gamma_{th_i}) = 1 - \exp\left(-\frac{\gamma_{th_i}}{\Omega_{C_{\text{in}}}}\right), \tag{21}$$

where $\Omega_{A_i} = \rho\Omega_{1,D_i}, \Omega_{B_n} = \rho\Omega_{BSUAV_{n^*}}, \Omega_{C_{\text{in}}} = \rho\Omega_{UAV_{n^*}D_i}$ represent the average SNR of the links, respectively. According to the NOMA principle, one outage event happens if there is indirect transmission or no successful forward sending. Hence, the OP at D_1 is given by

$$\begin{aligned} P_{D_1} = \Pr(\gamma_{D_1} < \gamma_{th_1}) &= \Pr\left(\max\left[\gamma_{1,D_1}, \gamma_{UAV_nD_1}\right] < \gamma_{th_1}\right) \\ &= \Pr(\gamma_{1,D_1} < \gamma_{th_1}, \gamma_{UAV_nD_1} < \gamma_{th_1}) \\ &= \underbrace{F_{\gamma_{1,D_1}}(\gamma_{th_1})}_{I_1} \underbrace{F_{\gamma_{UAV_{n*}D_1}}(\gamma_{th_1})}_{I_2}. \end{aligned} \tag{22}$$

Theorem 1 The OP at D_1 can be derived as (see (23)).

$$P_{D_i} = \left(1 - \exp\left[-\frac{\tilde{\gamma}_{th_1}}{\Omega_{A_1}}\right]\right)\left(1 - \sum_{n=1}^{N}\binom{N}{n}(-1)^{n-1}\exp\left[-\sigma\left(\frac{nG_E}{\Omega_{B_n}} + \frac{1}{\Omega_{C_{1n}}}\right)\right] 2\sqrt{\alpha}K_1(2\sqrt{\alpha})\right), \tag{23}$$

where $K_1(.)$ denotes the first-order modified Bessel function of the second kind ([34], Eq.(3.324.1)), $\alpha = ((n\sigma(1 + \sigma G_E))/(\Omega_{B_n}\Omega_{C_{1n}}))$, $\sigma = ((\gamma_{th_1})/(a_1G_E - a_2G_E\gamma_{th_1}))$, and $\sigma = ((\gamma_{th_1})/(a_1G_E - a_2G_E\gamma_{th_1}))$ with $a_1 > a_2\gamma_{th1}$.

Proof. See Appendix A. □

3.1.2. Outage Probability at D_2. Because D_2 needs to decode the signal of the first D_1, D_2 will be outage if both the first and the second stage are outages. Therefore, OP at D_2 can be formatted as

$$P_{D_2} = F_{\gamma_{1,D_2}}(\gamma_{th_2}) F_{\gamma_{UAV_{n*}D_2}}(\gamma_{th_2}). \tag{24}$$

Theorem 2 The OP at D_2 can be derived as (see (25)).

$$P_{D_2} = \left(1 - \exp\left[-\frac{\theta}{\Omega_{A_2}}\right]\right)\left(1 - \sum_{n=1}^{N}\binom{N}{n}(-1)^{n-1}\exp\left[-\omega\left(\frac{nG_E}{\Omega_{B_n}} + \frac{1}{\Omega_{B_n}}\right)\right] 2\sqrt{\beta}K_1(2\sqrt{\delta})\right), \tag{25}$$

where $K_1(.)$ denotes the first-order modified Bessel function of the second kind ([34], Eq.(3.324.1)), $\delta = ((n\omega(1 + \omega G_E))/(\Omega_{B_n}\Omega_{C_{2n}}))$, $\lambda_1 = ((\gamma_{th_2})/(a_1G_E - a_2G_E\gamma_{th_2}))$, $\lambda_2 = ((\gamma_{th_2})/(a_2G_E))$, and $\omega = \max(\lambda_1, \lambda_2)$ with $a_1 > a_2\gamma_{th1}$.

Proof. See Appendix B. □

3.1.3. Asymptotic Outage Probability at D_1. Applying the McLaurin expression, we get that $e^x \simeq 1 + x$ and $K_1(x) \simeq x^{-1}$ for small x. Hence, it turns out that

$$2\sqrt{\alpha}K_1(2\sqrt{\alpha}) \simeq 1. \tag{26}$$

An expression for the asymptotic OP for P_{D_1}, whose exact analysis is presented in (23), is simplified as follows:

$$1 - \exp\left(-\frac{\gamma_{th_1}}{\left(a_1 - a_2\gamma_{th_1}\right)\Omega_{A_1}}\right) = \frac{\tilde{\gamma}_{th_1}}{\Omega_{A_1}}, \tag{27}$$

$$\exp\left[-\sigma\left(\frac{nG_E}{\Omega_{B_n}} + \frac{1}{\Omega_{C_{1n}}}\right)\right] \simeq 1 - \sigma\left(\frac{kG_E}{\Omega_{B_n}} + \frac{1}{\Omega_{C_{1n}}}\right). \tag{28}$$

Hence, we can obtain a fraction of the asymptotic approximation for P_{D_1} in (24) as follows:

$$\begin{aligned} \tilde{M_1} \simeq 1 - \sum_{n=1}^{N}\binom{N}{n}(-1)^{n-1}\left[1 - \sigma\left(\frac{kG_E}{\Omega_{B_n}} + \frac{1}{\Omega_{C_{1n}}}\right)\right] = 1 \\ - \sum_{n=1}^{N}\binom{N}{n}(-1)^{n-1} + \sum_{k=1}^{N}\binom{N}{n}(-1)^{n-1} \times \sigma\left(\frac{nG_E}{\Omega_{B_n}} + \frac{1}{\Omega_{C_{1n}}}\right). \end{aligned} \tag{29}$$

With $\sum_{n=1}^{N}\binom{N}{n}(-1)^{n-1} = 1$.

We have

$$M_1 \simeq \left[\sum_{n=1}^{N}\binom{N}{n}(-1)^{n-1}\sigma\left(\frac{n}{\Omega_{B_n}} + \frac{1}{\Omega_{C_{1n}}}\right)\right]. \tag{30}$$

Table 2: Simulation parameters.

Parameters	Value
The standardized distance between the BS and UAV_n	$d = 0.3$
The path-loss factor	$m = 2$
The target rate	$R_1 = 0.5, R_2 = 0.25$
Energy harvesting efficiency	$\eta = 0.8$
Power splitting ratio	$\beta = 0.7$
Power allocation coefficient for signal	a_1=0.8, a_2=0.2

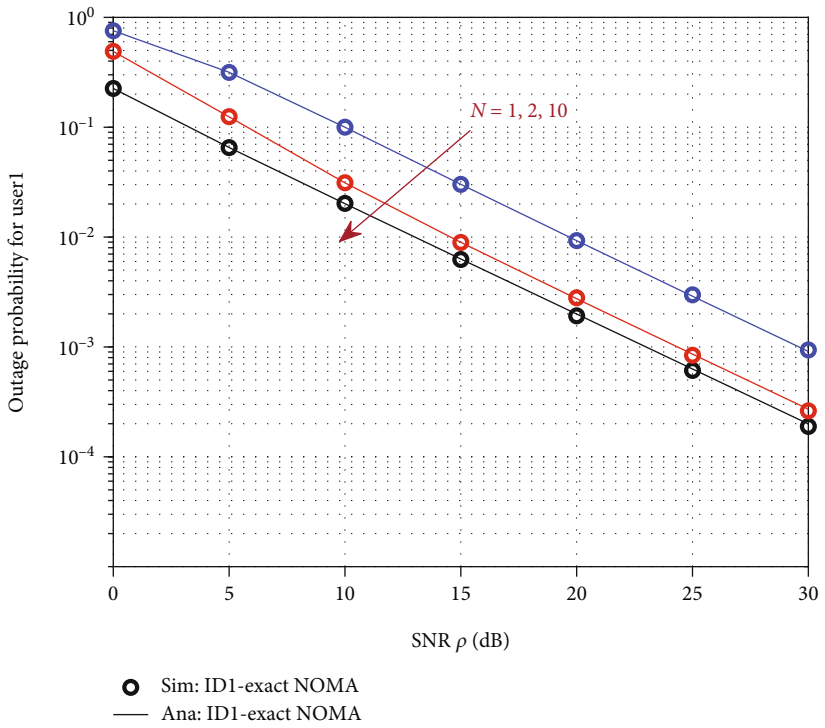

Figure 3: Outage probability at D_1 of PSR versus $N = \{1, 2, 10\}$ without a direct link.

Ultimately, from (31) and (34), an asymptotic OP expression for P_{D_1} in (25), we obtain

$$P_{D_1}^{\infty} = \frac{\tilde{\gamma}_{th_1}}{\Omega_{A_1}} M_1. \tag{31}$$

3.1.4. Asymptotic Outage Probability at D_2. The asymptotic OP for P_{D_2} is expressed the same as P_{D_1}, whose exact analysis is portrayed in (27); we have

$$1 - \exp\left(-\frac{\gamma_{th_2}}{\left(a_1 - a_2\gamma_{th_2}\right)\Omega_{A_2}}\right) = \frac{\tilde{\gamma}_{th_2}}{\Omega_{A_2}}, \tag{32}$$

$$\exp\left[-\omega\left(\frac{nG_E}{\Omega_{B_n}} + \frac{1}{\Omega_{C_{2n}}}\right)\right] \simeq 1 - \omega\left(\frac{nG_E}{\Omega_{B_n}} + \frac{1}{\Omega_{C_{2n}}}\right). \tag{33}$$

Thus, we can obtain a portion of the asymptotic approximation for P_{D_2} in (28) as follows:

$$\tilde{M}_2 \simeq 1 - \sum_{n=1}^{N} \binom{N}{n} (-1)^{n-1} \left[1 - \omega\left(\frac{nG_E}{\Omega_{B_n}} + \frac{1}{\Omega_{C_{2n}}}\right)\right] = 1 - \sum_{n=1}^{N} \binom{N}{n} (-1)^{n-1} + \sum_{n=1}^{N} \binom{N}{n} (-1)^{n-1} \times \omega\left(\frac{nG_E}{\Omega_{B_n}} + \frac{1}{\Omega_{C_{2n}}}\right). \tag{34}$$

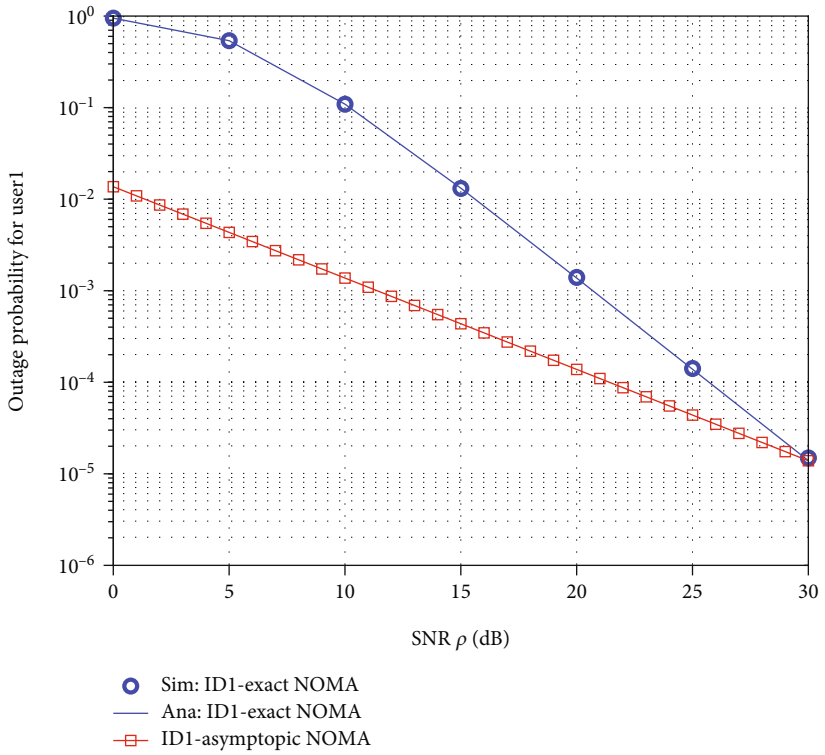

FIGURE 4: Outage probability at D_1 of PSR versus $N = 1$ with direct link.

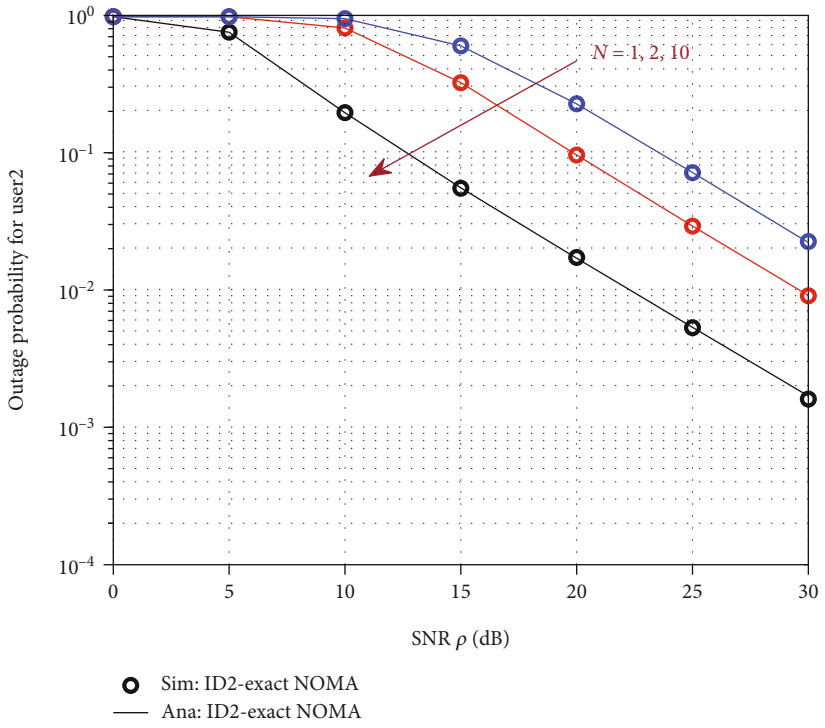

FIGURE 5: Outage probability at D_2 of PSR versus $N = \{1, 2, 10\}$ without a direct link.

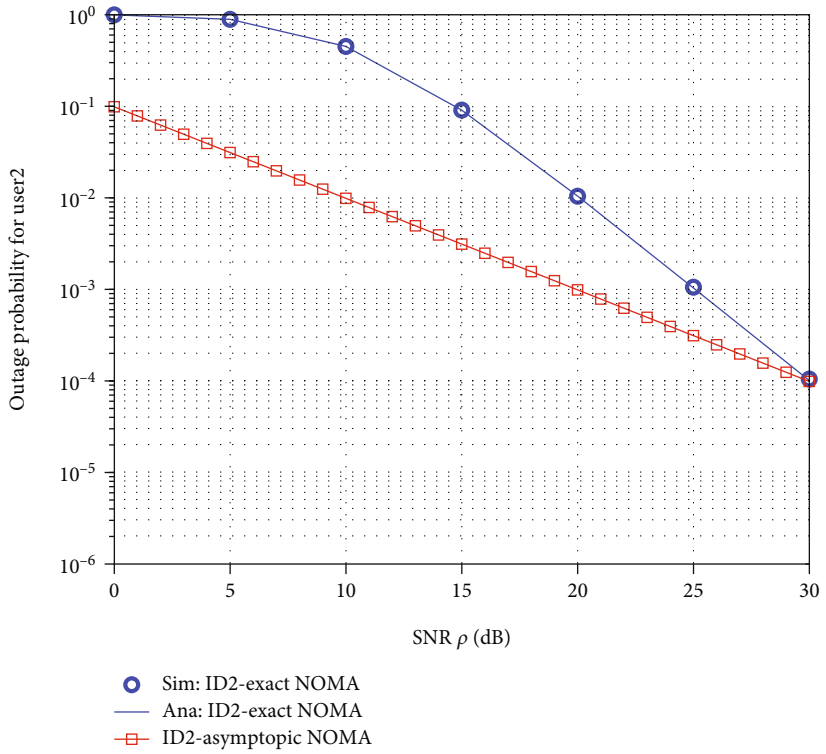

Figure 6: Outage probability at D_2 of PSR versus $N = 1$ with direct link.

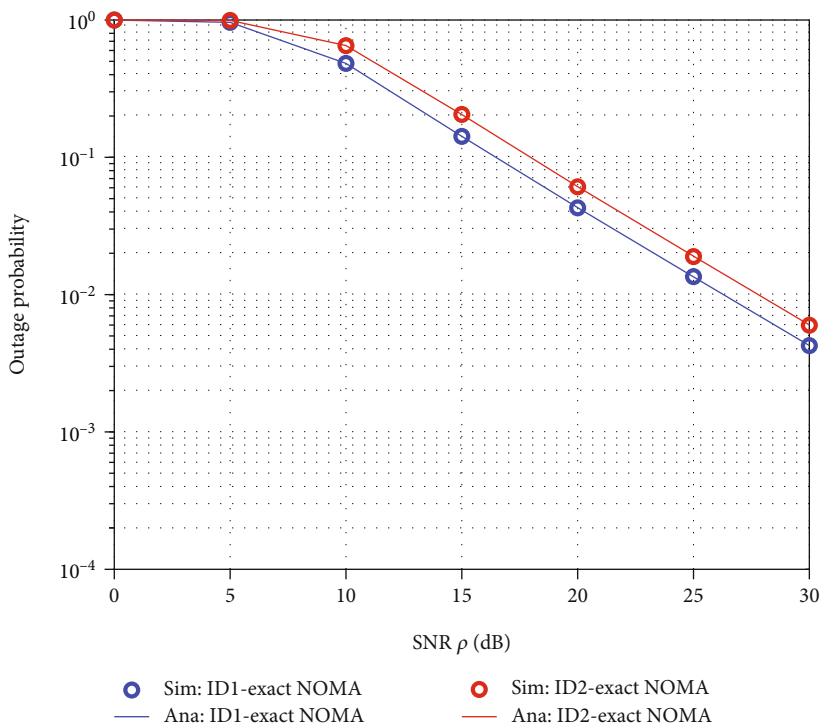

Figure 7: Outage probability at two IDs D_1 and D_2 of PSR versus $N = 3$ without direct link.

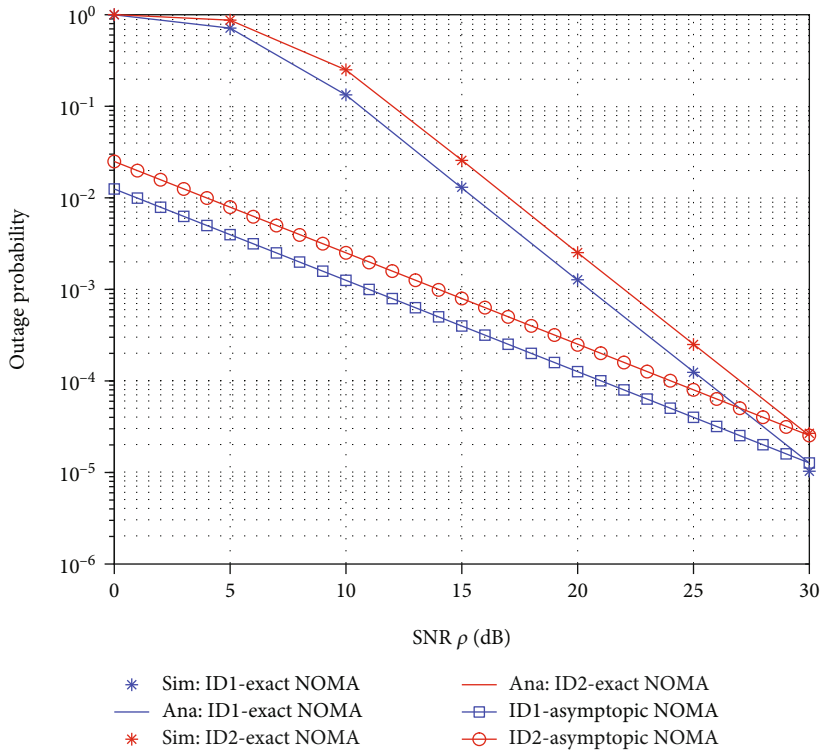

Figure 8: Outage probability at two IDs D_1 and D_2 of PSR versus $N = 3$ with direct link.

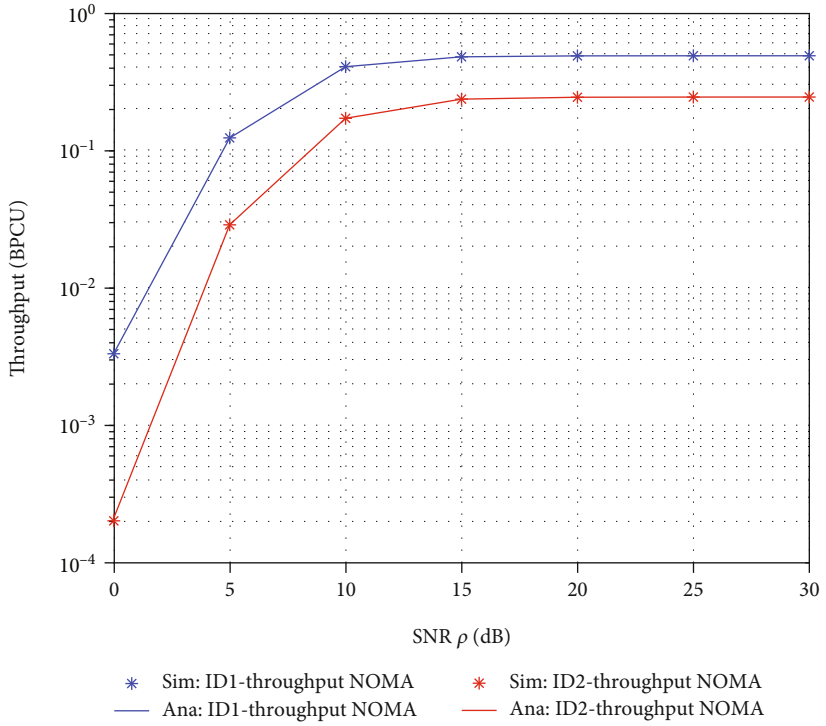

Figure 9: Throughput of two IDs D_1 and D_2 versus $N = 3$ with direct link.

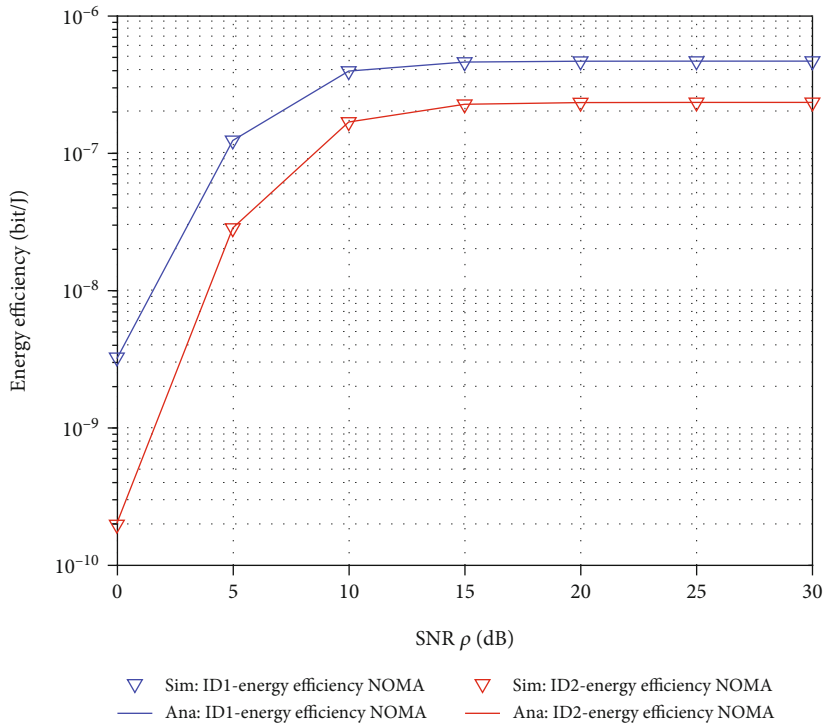

FIGURE 10: Energy efficiency of two IDs D_1 and D_2 versus $N = 3$ with direct link.

With $\sum_{n=1}^{N}\binom{N}{n}(-1)^{n-1} = 1$, we have,

$$M_2 \simeq \left[\sum_{n=1}^{N}\binom{N}{n}(-1)^{n-1}\omega\left(\frac{nG_E}{\Omega_{B_n}} + \frac{1}{\Omega_{C_{2n}}}\right)\right]. \tag{35}$$

Ultimately, from (36) and (39), an asymptotic OP expression for P_{D_2} in (29), we have

$$P_{D_2}^{\infty} = \frac{\theta}{\Omega_{A_2}} M_2. \tag{36}$$

3.2. System Throughput. In this case, the BS sends information at a constant target rate, rely on the performance of the OP because of the wireless fading channel. The system throughput of the NOMA indirect link is shown by as follows.

3.3. The System Throughput at D_1.

$$\tau_{D_1} = \left(1 - P_{D_1}\right)R_1, \tag{37}$$

where P_{D_1} is given in (23).

3.4. The System Throughput at D_2.

$$\tau_{D_2} = \left(1 - P_{D_2}\right)R_2, \tag{38}$$

where P_{D_2} is given in (25).

3.5. Energy Efficiency. EE is known as the ratio of sum throughput to total power consumed in the whole network system.

3.5.1. Energy Efficiency at D_1.

$$EE_{D_1} = \frac{2\tau_{D_1}}{\rho\left(1 + G_E\,\Omega_{Y_n}\right)}, \tag{39}$$

where τ_{D_1} is calculated by using (37).

3.5.2. Energy Efficiency at D_2.

$$EE_{D_2} = \frac{2\tau_{D_2}}{\rho\left(1 + G_E\,\Omega_{Y_n}\right)}, \tag{40}$$

where τ_{D_2} is calculated by using (38).

4. Simulation Results

This section confirms the derived analytical results shown by the previous sections. The distance between BS and IDs is standardized to unity, i.e., $\Omega_{BS->D_i} \approx 1$, $\Omega_{BS->R_n} \approx d^{-m}$, and $\Omega_{R_n->D_i} \approx (1-d)^{-m}$. Table 2 lists the simulation parameters

for assessment circumstances of the SWIPT based on multi-UAV cooperative NOMA systems.

Figure 3 describes the OP at D_1 with PSR protocol versus SNR without a direct link. Theoretically correct curves for the OP at D_1 for NOMA are plotted according to the corresponding points (3.24) and (3.27). Exact probability curves are consistent with Monte-Carlo simulation results. The value ID_1 is assumed to be $N = \{1, 2, 10\}$, and $\Omega_{SD_1} = 0$.

Figure 4 shows the OP at D_1 with PSR protocol versus SNR with direct link. Theoretically correct curves for the OP at ID_1 for NOMA are plotted according to the corresponding points (3.24), (3.27), and (3.37). Assume that the value ID_1 is $N = 1$ and $\Omega_{SD_1} = 1$.

Figure 5 describes the OP at D_2 with PSR protocol versus SNR indirect link. Theoretically correct curves for the OP of D_2 for NOMA are plotted according to the corresponding points (3.24) and (3.27). Exact probability curves are consistent with Monte-Carlo simulation results. The value ID_2 is assumed to be $N = \{1, 2, 10\}$, and $\Omega_{SD_1} = 0$.

Figure 6 shows the OP at D_2 with PSR protocol versus SNR with direct link. Theoretically correct curves for the OP at ID_2 for NOMA are plotted according to the corresponding Equations (3.24), (3.27), and (3.37). Assume that the value ID_2 is $N = 1$ and $\Omega_{SD_1} = 1$.

Figure 7 shows the OP at D_1 and D_2 with PSR protocol versus SNR indirect link. Theoretically correct curves for the OPs at D_1 and D_2 for NOMA are plotted according to the Equations (3.24), (3.27), (3.28), and (3.30), respectively. The values at D_1 and D_2 are assumed $N = 3$, and $\Omega_1 = \Omega_1 = 0$.

Figure 8 depicts the OP at D_1 and D_2 of PSR protocol versus SNR indirect link. Assume that the values at D_1 and D_2 are $N = 3$ and $\Omega_{SD_1} = \Omega_{SD_2} = 1$.

Figure 9 shows the throughput at D_1 and D_2 of PSR protocol versus SNR with direct link. Theoretically correct curves for the throughput at D_1 and D_2 for NOMA are plotted according to the Equations (3.43) and (3.44). Throughput curves are consistent with the results of the Monte-Carlo simulation. The values at D_1 and D_2 are assumed $N = 3$, and $\Omega_{SD_1} = \Omega_{SD_2} = 1$.

Figure 10 shows the energy efficiency at D_1 and D_2 of PSR protocol versus SNR with direct link. The theoretically correct curves for the energy efficiency at D_1 and D_2 for NOMA are plotted according to the points (3.45) and (3.46). Energy efficiency curves consistent with Monte-Carlo simulation results. Assume that the values at D_1 and D_2 are $N = 3$ and $\Omega_{SD_1} = \Omega_{SD_2} = 1$.

5. Conclusion

This paper has investigated the BS-based PSR protocol for the NOMA system. We used an AF rotary-wing relay network with cooperative UAV systems with UAV options. Closed-form expressions of OP for the two IDs were derived. Based on a simulation of the OP, throughput, EE, the results indicated that NOMA with the UAV option improves the efficiency increase by increasing the number of UAVs, but hardly any outage performance when the number of UAVs increases from 2 to 10 in the high SNR region. The indicates that the NOMA protocol with the UAVO will not need to use more than two UAVs. Numerical results confirm that our derived analytical results matched precisely with the Monte-Carlo simulation results in connection with all possible system parameters. Furthermore, we also can deploy the multiple antennas system at two IDs along with the investigation of Rayleigh Rician fading channel for enhancing the system performance that would be in our future works.

Appendix

A. Proof of Theorem 1

According to (22), the OP of D_1 for NOMA can be calculated as follows:

$$\begin{aligned} I_1 &= F_{\gamma_{1,D_1}}\left(\gamma_{th_1}\right) = \Pr\left(\frac{a_1 A_1}{a_2 A_1 + 1} < \gamma_{th_1}\right) \\ &= \Pr\left(a_1 A_1 - a_2 A_1 \gamma_{th_1} < \gamma_{th_1}\right) = \Pr\left(A_1 < \frac{\gamma_{th_1}}{a_1 - a_2 \gamma_{th_1}}\right) \\ &= 1 - \exp\left(-\frac{\tilde{\gamma}_{th_1}}{\Omega_{A_1}}\right). \end{aligned} \tag{A.1}$$

Put $\tilde{\gamma}_{th_1} = \gamma_{th_1}/a_1 - a_2\gamma_{th_1}$.

Similar to prove I_1, the calculation process of I_2 is presented as (see(A.2)):

$$\begin{aligned} I_2 &= F_{\gamma_{R_{n*}D_1}}\left(\gamma_{th_1}\right) = \Pr\left(\frac{a_1 B_{n*} C_{1n*}}{a_2 B_{n*} C_{1n*} + B_{n*} + C_{1n*} + 1} < \gamma_{th_1}\right) = F_{C_{1n*}}(\sigma) \\ &\quad + \int_{\sigma}^{+\infty}\left[1 - \sum_{n=1}^{N}\binom{N}{n}(-1)^{n-1}\exp\left(-\frac{n}{\Omega_{B_n}}\left(\frac{\sigma(c+1)}{c-\sigma}\right)\right)\right] f_{C_{1n*}}(c)dc \\ &= 1 - \sum_{n=1}^{N}\binom{N}{n}(-1)^{n-1}\frac{1}{\Omega_{C_{1n}}}\int_{\sigma}^{+\infty}\exp\left(-\frac{n}{\Omega_{B_n}}\left(\frac{\sigma(cG_E+1)}{c-\sigma}\right)\right)\exp \\ &\quad \cdot\left(-\frac{c}{\Omega_{C_{1n}}}\right)dc = 1 - \sum_{n=1}^{N}\binom{N}{n}(-1)^{n-1}\exp \\ &\quad \cdot\left[-\sigma\left(\frac{nG_E}{\Omega_{B_n}} + \frac{1}{\Omega_{C_{1n}}}\right)\right] 2\sqrt{\alpha}K_1\left(2\sqrt{\alpha}\right) = F_{C_{1n*}}(\sigma) + \int_{\sigma}^{+\infty} \\ &\quad \cdot\left[1 - \sum_{n=1}^{N}\binom{N}{n}(-1)^{n-1}\exp\left(-\frac{n}{\Omega_{B_n}}\left(\frac{\sigma(c+1)}{c-\sigma}\right)\right)\right] f_{C_{1n*}}(c)dc \\ &= 1 - \sum_{n=1}^{N}\binom{N}{n}(-1)^{n-1}\frac{1}{\Omega_{C_{1n}}}\int_{\sigma}^{+\infty}\exp\left(-\frac{n}{\Omega_{B_n}}\left(\frac{\sigma(cG_E+1)}{c-\sigma}\right)\right)\exp \\ &\quad \cdot\left(-\frac{c}{\Omega_{C_{1n}}}\right)dc = 1 - \sum_{n=1}^{N}\binom{N}{n}(-1)^{n-1}\exp \\ &\quad \cdot\left[-\sigma\left(\frac{nG_E}{\Omega_{B_n}} + \frac{1}{\Omega_{C_{1n}}}\right)\right] 2\sqrt{\alpha}K_1\left(2\sqrt{\alpha}\right). \end{aligned} \tag{A.2}$$

Put $\alpha = ((n\sigma(1+\sigma G_E))/(\Omega_{B_n}\Omega_{C_{1n}}))$, $\sigma = ((\gamma_{th_1})/(a_1 G_E - a_2 G_E \gamma_{th_1}))$, and $\sigma = ((\gamma_{th_1})/(a_1 G_E - a_2 G_E \gamma_{th_1}))$ with $a_1 > a_1$

γ_{th1}, and $K_1(.)$ denotes the first-order modified Bessel function of the second kind [38, $Eq.(3.324.1)$]. By substituting (A.1) and (A.1) into (22), the theorem is proved.

B. Proof of Theorem 2

According to (26), the OP at D_2 for NOMA is calculated as follows:

$$\begin{aligned} F_{\gamma_{1,D_2}}\left(\gamma_{th_2}\right) &= \Pr\left(\frac{a_1A_2}{a_2A_2+1} < \gamma_{th_2}, a_2A_2 < \gamma_{th_2}\right) \\ &= \Pr\left(A_2 < \tilde{\gamma_{th_2}}, A_2 < \gamma'_{th_2}\right) \\ &= \Pr\left(A_2 < \max\left[\tilde{\gamma_{th_2}}, \gamma'_{th_2}\right]\right) \\ &= 1 - \exp\left(-\frac{\theta}{\Omega_{A_2}}\right). \end{aligned} \tag{B.1}$$

Put $\theta = \max(\gamma_{th_2}\tilde{}, \gamma'_{th_2})$, $\gamma'_{th_2} = \gamma_{th_2}/a_2$, and $\gamma_{th_2}\tilde{} = \gamma_{th_2}/(a_1 - a_2\gamma_{th_2})$.

Similarly, we have (see(B.2))

$$\begin{aligned} F_{\gamma_{R_{n*}D_2}}\left(\gamma_{th_2}\right) &= \Pr\left(\frac{a_1B_{n*}C_{2n*}G_E}{a_2B_{n*}C_{2n*}G_E + B_{n*} + C_{2n*}G_E + 1} < \gamma_{th_2}, \right. \\ &\quad \left. \cdot \frac{a_2B_{n*}C_{2n*}G_E}{Y_{n*} + C_{2n*}G_E + 1} < \gamma_{th_2}\right) \\ &= \Pr\left(B_{n*} < \frac{C_{2n*}+1}{C_{2n*}/\lambda_1 - 1}, Y_{n*} < \frac{C_{2n*}+1}{C_{2n*}/\lambda_2 - 1}\right) \\ &= \Pr\left(Y_{n*} < \frac{C_{2n*}+1}{C_{2n*}/\omega - 1}\right) = F_{C_{2n*}}(\omega) + \int_{C_2}^{+\infty} F_{B_{n*}} \\ &\quad \cdot \left(\frac{\omega(c+1)}{c-\omega}\right) f_{C_{2n*}}(c)dc = F_{C_{2n*}}(\omega) + \int_{\omega}^{+\infty} \\ &\quad \cdot \left[1 - \sum_{n=1}^{N}\binom{N}{n}(-1)^{n-1}\exp\left(-\frac{n}{\Omega_{B_n}}\left(\frac{\omega(c+1)}{c-\omega}\right)\right)\right] f_{C_{2n*}}(c)dc \\ &= 1 - \sum_{n=1}^{N}\binom{N}{n}(-1)^{n-1}\frac{1}{\Omega_{C_{2n}}}\int_{\omega}^{+\infty}\exp\left(-\frac{n}{\Omega_{B_n}}\left(\frac{\omega(c+1)}{c-\omega}\right)\right)\exp \\ &\quad \cdot \left(-\frac{c}{\Omega_{C_{2k}}}\right)dc = 1 - \sum_{n=1}^{N}\binom{N}{n}(-1)^{n-1}\exp \\ &\quad \cdot \left[-\omega\left(\frac{nG_E}{\Omega_{B_n}} + \frac{1}{\Omega_{C_{2n}}}\right)\right] 2\sqrt{\beta}K_1\left(2\sqrt{\beta}\right). \end{aligned} \tag{B.2}$$

Put $\delta = ((n\omega(1+\omega G_E))/(\Omega_{B_n}\Omega_{C_{2n}}))$, $\lambda_1 = ((\gamma_{th_2})/(a_1G_E - a_2G_E\gamma_{th_2}))$, and $\lambda_2 = ((\gamma_{th_2})/(a_2G_E))$, $\omega = \max(\lambda_1, \lambda_2)$.

By replacing (B.1) and (B.2) into (26), the expression of (26) is obtained. This completes the proof.

Data Availability

The data used to support the findings of this study are included in the paper.

Conflicts of Interest

Authors declare there is no conflict of interest in this manuscript.

References

[1] P. K. Sharma and D. I. Kim, "UAV-enabled downlink wireless system with non-orthogonal multiple access," in *IEEE Globecom Workshops (GC Wkshps)*, Singapore, 2017.

[2] Y. Liu, Z. Qin, Y. Cai, Y. Gao, G. Y. Li, and A. Nallanathan, "UAV communications based on non-orthogonal multiple access," *IEEE Wireless Communications*, vol. 26, no. 1, pp. 52–57, 2019.

[3] B. Li, Z. Fei, and Y. Zhang, "UAV communications for 5G and beyond: recent advances and future trends," *IEEE Internet of Things Journal*, vol. 6, no. 2, pp. 2241–2263, 2019.

[4] M. Mozaffari, W. Saad, M. Bennis, Y. H. Nam, and M. Debbah, "A tutorial on UAVs for wireless networks: applications, challenges, and open problems," *IEEE communications surveys & tutorials*, vol. 21, no. 3, pp. 2334–2360, 2019.

[5] S. T. Ooi, R. Ngah, and M. H. Azmi, "Full-duplex user-centric communication using non-orthogonal multiple access," *TELKOMNIKA (Telecommunication Computing Electronics and Control)*, vol. 17, no. 5, pp. 2169–2178, 2019.

[6] S. R. Islam, N. Avazov, O. A. Dobre, and K. S. Kwak, "Power-domain non-orthogonal multiple access (NOMA) in 5G systems: potentials and challenges," *IEEE Communications Surveys Tutorials*, vol. 19, no. 2, pp. 721–742, 2017.

[7] H. Q. Tran, T. T. Nguyen, C. V. Phan, and Q. T. Vien, "Power-splitting relaying protocol for wireless energy harvesting and information processing in NOMA systems," *IET Communications*, vol. 13, no. 14, pp. 2132–2140, 2019.

[8] H. Q. Tran, C. V. Phan, and Q. T. Vien, "Power splitting versus time switching based cooperative relaying protocols for SWIPT in NOMA systems," *Physical Communication*, vol. 41, article 101098, 2020.

[9] H. Q. Tran, C. V. Phan, and Q. T. Vien, "Performance analysis of power-splitting relaying protocol in SWIPT based cooperative NOMA systems," *EURASIP Journal on Wireless Communications and Networking*, vol. 2021, 26 pages, 2021.

[10] H. Q. Tran, "Two energy harvesting protocols for SWIPT at UAVs in cooperative relaying networks of IoT systems," *Wireless Personal Communications*, vol. 122, no. 4, pp. 3719–3740, 2022.

[11] B. Di, L. Song, Y. Li, and G. Y. Li, "NOMA-based low-latency and high-reliable broadcast communications for 5G V2X services," in *GLOBECOM 2017-2017 IEEE Global Communications Conference*, pp. 1–6, Singapore, 2017.

[12] Y. Saito, Y. Kishiyama, A. Benjebbour, T. Nakamura, A. Li, and K. Higuchi, "Non-orthogonal multiple access (NOMA) for cellular future radio access," in *2013 IEEE 77th vehicular technology conference (VTC Spring)*, pp. 1–5, Dresden, Germany, 2013.

[13] K. Higuchi and A. Benjebbour, "Non-orthogonal multiple access (NOMA) with successive interference cancellation for future radio access," *IEICE Transactions on Communications*, vol. E98.B, no. 3, pp. 403–414, 2015.

[14] A. A. Nasir, H. D. Tuan, T. Q. Duong, and H. V. Poor, "UAV-enabled communication using NOMA," *IEEE Transactions on Communications*, vol. 67, no. 7, pp. 5126–5138, 2019.

[15] J. Lu, Y. Wang, T. Liu et al., "UAV-enabled uplink non-orthogonal multiple access system: joint deployment and power control," *IEEE Transactions on Vehicular Technology*, vol. 69, no. 9, pp. 10090–10102, 2020.

[16] X. Mu, Y. Liu, L. Guo, and J. Lin, "Non-orthogonal multiple access for air-to-ground communication," *IEEE Transactions on Communications*, vol. 68, no. 5, pp. 2934–2949, 2020.

[17] P. N. Son, H. Y. Kong, and A. Anpalagan, "Exact outage analysis of a decode-and-forward cooperative communication network with N th best energy harvesting relay selection," *Annales des Telecommunications*, vol. 71, no. 5-6, pp. 251–263, 2016.

[18] A. A. Nasir, X. Zhou, S. Durrani, and R. A. Kennedy, "Relaying protocols for wireless energy harvesting and information processing," *IEEE Transactions on Wireless Communications*, vol. 12, no. 7, pp. 3622–3636, 2013.

[19] D. Deng and Q. Zhou, "Outdated relay selection for UAV-enabled networks with cooperative NOMA," *Physical Communication*, vol. 32, pp. 112–119, 2019.

[20] N. Zhao, W. Lu, M. Sheng et al., "UAV-assisted emergency networks in disasters," *Telkomnika*, vol. 26, no. 1, pp. 45–51, 2019.

[21] H. Zhang, B. Wang, C. Chen, X. Cheng, and H. Li, "Resource allocation in UAV-NOMA communication systems based on proportional fairness," *Journal of Communications and Information Networks*, vol. 5, no. 2, pp. 111–120, 2020.

[22] Q. Wu, Y. Zeng, and R. Zhang, "Joint trajectory and communication design for multi-UAV enabled wireless networks," *IEEE Transactions on Wireless Communications*, vol. 17, no. 3, pp. 2109–2121, 2018.

[23] Y. Zeng, Q. Wu, and R. Zhang, "Accessing from the sky: a tutorial on UAV communications for 5G and beyond," *Proceedings of the IEEE*, vol. 107, no. 12, pp. 2327–2375, 2019.

[24] Y. Liu, S. Zhang, X. Mu et al., "Evolution of NOMA toward next generation multiple access (ngma) for 6G," *IEEE Journal on Selected Areas in Communications*, vol. 40, no. 4, pp. 1037–1071, 2022.

[25] T. Z. Ernest, A. S. Madhukumar, R. P. Sirigina, and A. K. Krishna, "NOMA-aided UAV communications over correlated Rician shadowed fading channels," *IEEE Transactions on Signal Processing*, vol. 68, pp. 3103–3116, 2020.

[26] X. Li, Q. Wang, Y. Liu, T. A. Tsiftsis, Z. Ding, and A. Nallanathan, "UAV-aided multi-way NOMA networks with residual hardware impairments," *IEEE Wireless Communications Letters*, vol. 9, no. 9, pp. 1538–1542, 2020.

[27] T. M. Hoang, B. C. Nguyen, L. T. Dung, and T. Kim, "Outage performance of multi-antenna mobile UAV-assisted NOMA relay systems over Nakagami-m Fading channels," *IEEE Access*, vol. 8, pp. 215033–215043, 2020.

[28] X. Liu and X. Zhang, "Rate and energy efficiency improvements for 5G-based IoT with simultaneous transfer," *IEEE Internet of Things Journal*, vol. 6, no. 4, pp. 5971–5980, 2019.

[29] D. H. Tran, V. D. Nguyen, S. Chatzinotas, T. X. Vu, and B. Ottersten, "UAV relay-assisted emergency communications in IoT networks: resource allocation and trajectory optimization," *IEEE Transactions on Wireless Communications*, vol. 21, no. 3, pp. 1621–1637, 2021.

[30] H. Li, J. Li, M. Liu, Z. Ding, and F. Gong, "Energy harvesting and resource allocation for cache-enabled UAV based IoT NOMA networks," *IEEE Transactions on Vehicular Technology*, vol. 70, no. 9, pp. 9625–9630, 2021.

[31] S. Yin, Y. Zhao, and L. Li, "UAV-assisted cooperative communications with power-splitting SWIPT," in *2018 IEEE International Conference on Communication Systems (ICCS)*, pp. 162–167, Chengdu, China, 2018.

[32] A. N. Nguyen, V. N. Vo, C. So-in, and D. B. Ha, "System performance analysis for an energy harvesting IoT system using a DF/AF UAV-enabled relay with downlink NOMA under Nakagami-m fading," *Sensors*, vol. 21, no. 1, p. 285, 2021.

[33] S. Lee, D. B. Costa, Q.-T. Vien, T. Q. Duong, and R. T. Sousa Jr., "Non-orthogonal multiple access schemes with partial relay selection," *IET Communications*, vol. 11, no. 6, pp. 846–854, 2017.

[34] I. S. Gradshteyn and I. M. Ryzhik, *Table of Integrals, Series and Products*, Academic Press, San Diego, CA, 7th edition, 2007.